2010

Dynamic conductivity of graphene with electron-LO-phonon interaction

Anthony Wright
University of Wollongong, arw75@uow.edu.au

Chao Zhang
University of Wollongong, czhang@uow.edu.au

Publication Details

Wright, A. and Zhang, C. (2010). Dynamic conductivity of graphene with electron-LO-phonon interaction. Physical Review B (Condensed Matter and Materials Physics), 81 (16), 165413-1-165413-7.

Dynamic conductivity of graphene with electron-LO-phonon interaction

A. R. Wright and C. Zhang
School of Engineering Physics, University of Wollongong, Wollongong, New South Wales 2522, Australia
(Received 3 November 2009; revised manuscript received 17 March 2010; published 8 April 2010)

We calculate the electrical conductivity of single-layer graphene within the regime of massless Dirac fermions. We consider the electron-LO-phonon interactions as the dominant scattering mechanism. By using the Green's-function method, we are able to obtain the quantitative contribution from the five leading diagrams in the high-frequency approximation. It is found that electron-LO-phonon interactions cause an increase to the electromagnetic absorption of single-layer graphene of as much as 20% at room temperature. The spectrum is dominated by a continuum contribution with a peak at $\omega=\omega_{\mathrm{LO}}/2$ and represents intraband transitions. The temperature and doping dependence of these peak corrections is also investigated. These results probe the validity of the universal conductivity of graphene with respect to electron-phonon interactions under a range of conditions.

DOI: 10.1103/PhysRevB.81.165413 PACS number(s): 73.50.Mx, 78.66.−w, 81.05.U−

I. INTRODUCTION

Since the isolation of single layers of graphite in 2003,[1] a lot of exciting work on single-layer graphene has been done.[2] For example, the prediction and observation of electron-hole symmetry and a half-integer quantum Hall effect,[3–5] finite conductivity at zero charge-carrier concentration,[3] the strong suppression of weak localization,[6–8] and universal conductance.[9–11]

The "universal" conductance of graphene is a remarkable ac phenomenon. It is a direct result of the linear energy dispersion of graphene. Linear subbands imply both a constant density of states as well as consistent transition matrix elements, which means that for as long as the linear (Dirac) approximation is valid, the conductance is a constant. The value of the universal conductance of single-layer graphene is $\sigma_0=e^2/4\hbar$. This result is easily achieved by several methods. In particular, the Kubo formula yields this result when the interaction Hamiltonian is assumed to be negligible.

Deviations from universal conductance have been shown to occur due to variations in geometry,[12,13] field energy,[14,15] and field strength.[16,17] It need not be demonstrated that the effect of finite temperature on the distribution functions, as well as doping to create an effective band gap between available states, will also alter the value of σ_0, especially at lower energies.

In fact, the optical properties of graphene-based systems have become quite an active field of research. After the initial flurry of excitement that followed the demonstration of the universal conductivity at energies as high as the optical regime—a direct demonstration of the accuracy of the Dirac band structure—there has been increasing interest in graphene-based materials for photonic applications, as well as the realization of graphene's potential in the terahertz-far infrared (THz-FIR) regime, which have lead to some very interesting results. The optical properties of bilayer graphene have been studied extensively, both theoretically[13,18–20] and experimentally.[12,21] Bilayer graphene, while having a baseline optical conductivity of, unsurprisingly, $\sigma_{BLG}=2\sigma_0$, exhibits a much stronger response of $\sigma_{BLG}\approx 6\sigma_0-8\sigma_0$ at characteristic energies which are proportional to the interlayer coupling, $\gamma\approx 0.3$ eV.[13] When confining single-layer and bilayer graphene into pseudo-one-dimensional structures called graphene nanoribbons, the continuous optical conductivity has been found to disappear and the emergence of sharp resonant peaks are observed. These peaks are tunable by an external magnetic field,[22] and in the case of bilayer ribbons, a two order of magnitude increase in the THz-FIR conductivity has been predicted, and is tunable via a strong width dependence.[23]

This strong and varied optical activity, particularly in the THz-FIR regime, makes graphene-based materials potential candidates for future photonic applications. Returning to intrinsic single-layer graphene however, no such strong response has been predicted, except outside of the Dirac regime.[14] The continuum absorption due to the linear Dirac band structure, in general, remains. However, it has long been known that nonlinear effects in a material are absent if it has a strictly parabolic band structure. It has recently been shown that graphene's linear subband structure leads to a very strong nonlinear optical conductance, particularly at relatively low energies—the THz-FIR regime.[17] Furthermore, mechanical stretching has been shown to induce a strong transverse conductivity in graphene which can be as strong as $\sigma_{xy}\approx\sigma_0$ for quite low stretching amounts.[24]

With all these predictions having emerged, the optical properties of graphene-based systems appear to be more significant and more versatile than perhaps previously believed. However, a rather fundamental issue remains unsolved: What is the effect of electron-phonon coupling on these properties? Will the predicted properties remain at, say, room temperature?

With these questions in mind, we have investigated the impact of electron-phonon coupling on the ac conductivity of graphene-based systems. While these calculations are only strictly relevant for two-dimensional single-layer graphene, the results will inform our understanding of the contribution of electron-phonon interactions to the ac conductivity of graphene systems, in general, and serve as a starting point for further theoretical and experimental investigation.

In this paper, we evaluate the finite-temperature effect of the contribution to the optical conductivity obtained when electron-LO-phonon interactions are included in the optical

conductance calculation. Related work was previously done via corrections to the self-energy of the electron propagators.[25,26] These do not include exchange and correlation in the conductivity matrix elements but instead act as corrections to the electronic band structure. Here we will calculate the effects of exchange and correlation via a perturbation-theory expansion of the electron-phonon interaction Hamiltonian. The choice of which terms to include in the calculation will be determined diagrammatically with a simple high-frequency approximation. The electron-LO-phonon interaction contribution to the universal conductivity of graphene that we obtain is relatively small but becomes significant as temperature is sufficiently increased. Moreover, the nature of electron-LO-phonon interactions in graphene is further understood by these results.

II. THEORY

Let us consider low-energy electrons in graphene which are described by the massless Dirac Hamiltonian,

$$H = H_0 + H_I, \tag{1}$$

where H_0 is the Hamiltonian of noninteracting electrons and phonons,

$$H_0 = -v_F \sum_{\mathbf{k},s} k_s c^\dagger_{\mathbf{k},s} c_{\mathbf{k},-\mathbf{s}} + \sum_{\mathbf{q}} \omega_{\mathbf{q}} b^\dagger_{\mathbf{q}} b_{\mathbf{q}}. \tag{2}$$

Here $v_F = 3t/2$, where $t \approx 2.7$ eV is the first nearest-neighbor hopping amplitude, $s = \pm 1$, and $k_\pm = k_x \pm ik_y$, and $c_{\mathbf{k}}(b_{\mathbf{k}})$ is the electron (phonon) annihilation operator whose Hermitian conjugate is a creation operator, and ω_q is the LO-phonon frequency. H_I is the electron-LO-phonon interaction term,

$$H_I = \sum_{\mathbf{k},\mathbf{q},s,s'} F_{s,s'}(\mathbf{k},\mathbf{q}) M_q c^\dagger_{\mathbf{k}+\mathbf{q},s} c_{\mathbf{k},s'} (b_{\mathbf{q}} + b^\dagger_{-\mathbf{q}}), \tag{3}$$

where $F_{s,s'}(\mathbf{k},\mathbf{q})$ is the electron transition matrix element which will be calculated in due course, M_q is the electron-phonon coupling strength which, in the case of LO phonons, has no $\mathbf{q}$ dependence but is given by a constant. We shall neglect the spin degree of freedom in our calculation.

The single-particle eigenvalues and eigenvectors can be written as

$$\epsilon_{\mathbf{k},s} = s v_F |\mathbf{k}| \tag{4}$$

and

$$\psi_s(\mathbf{k}) = \frac{1}{\sqrt{2}} \begin{pmatrix} s e^{i\phi(\mathbf{k})} \\ 1 \end{pmatrix}, \tag{5}$$

where $\phi(\mathbf{k}) = \tan^{-1}(k_y/k_x)$. The corresponding fermion field operators have the form $\Psi_s(\mathbf{r}) = \Sigma_{\mathbf{k}} \psi_s(\mathbf{k}) e^{i\mathbf{k}\cdot\mathbf{r}} c_{\mathbf{k},s}$, from which the current operator is given as $j_\nu = e^2 \Sigma_{s,s',\mathbf{k},\mathbf{k}'} \langle \mathbf{k}', s' | \partial H_0 / \partial k_\nu | \mathbf{k}, s \rangle$.

The Kubo formula for electrical conductivity is given by[27]

$$\sigma_{\mu,\nu}(\mathbf{q},\omega) = \frac{1}{\omega} \int_0^\infty dt e^{i\omega t} \langle [j^\dagger_\mu(\mathbf{q},t), j_\nu(\mathbf{q},0)] \rangle. \tag{6}$$

The time dependence of an operator is given by $O(t) = e^{iHt} O e^{-iHt}$. In order to represent the Kubo formula in terms of Green's functions, we need to find the ensemble average with the complete ground state including interactions. So the current-current correlation function of Eq. (6) takes the form

$$M_{\mu\nu}(\mathbf{q},t) = \frac{1}{V} \langle T j^\dagger_\mu(\mathbf{q},t) j_\nu(\mathbf{q},0) \rangle, \tag{7}$$

where the required ground state cannot be determined analytically. Here T is the time-ordering operator. In the interaction picture, we describe our ground state without interactions and explicitly introduce interactions as a perturbation such that

$$M_{\mu\nu}(\mathbf{q},t) = \frac{1}{V} \frac{{}_0\langle T j^\dagger_\mu(\mathbf{q},t) U(\beta) j_\nu(\mathbf{q},0) \rangle_0}{{}_0\langle U(\beta) \rangle_0}, \tag{8}$$

where the subscript 0 implies the unperturbed ground state of Eq. (5). We now exploit the well-known existence of a Dyson's equation for the correlation function which simplifies our correlation function significantly such that

$$M_{\mu\nu}(\mathbf{q},t) = \frac{1}{V} {}_0\langle T j^\dagger_\mu(\mathbf{q},t) U(\beta) j_\nu(\mathbf{q},0) \rangle_0^{\text{connected}}, \tag{9}$$

where connected refers to the consideration of only connected Feynman diagrams. The interaction term $U(\beta)$ is

$$U(\beta) = \exp\left[-\int_0^\beta du H_I(u) \right]. \tag{10}$$

Writing out all terms explicitly, we have

$$\begin{aligned} M_{\mu\nu}(\mathbf{q},t) = \frac{1}{V} \sum_{\lambda_1,\lambda_2,\lambda_3,\lambda_4} \sum_{\mathbf{k},\mathbf{k}'} & v^*_{\mu,\lambda_1,\lambda_2}(\mathbf{p}+\mathbf{q}) v_{\nu,\lambda_3,\lambda_4}(\mathbf{p}) \\ & \times {}_0\langle T[c^\dagger_{\mathbf{p}+\mathbf{q},\lambda_1} c_{\mathbf{p},\lambda_2} (1 + H_I + H_I^2/2 \\ & + \cdots) c^\dagger_{\mathbf{p}+\mathbf{q},\lambda_3} c_{\mathbf{p},\lambda_4}] \rangle_0, \end{aligned} \tag{11}$$

where the integration over each interaction Hamiltonian is assumed, and $v_{\mu,i,j}(\mathbf{k}) = \langle \mathbf{k}, i | \partial H_0 / \partial k_\mu | \mathbf{k}, j \rangle$. In the expansion of the exponential, the term with no interaction is the single-loop optical conductivity which, in the case of Dirac graphene, yields the universal value $\sigma_0 = e^2/4h$. All higher-order terms are corrections due to the electron-phonon interaction $[\sigma_{eph}(\omega)]$, which we will choose a subclass of below. The total longitudinal optical conductivity of graphene then, is given by

$$\sigma_{xx(yy)}(\omega) = \sigma_0 + \sigma_{eph}(\omega) = \frac{e^2}{4h} + \sigma_{eph}(\omega). \tag{12}$$

From now on we will neglect the constant universal conductivity, and focus solely on the subclass of diagrams chosen to approximate $\sigma_{eph}(\omega)$.

Our system is isotropic, and so we will drop the indices μ, ν from now on, and expect the Hall contribution to be zero. The Green's function described above will give us the phonon contribution to the longitudinal conductivity of graphene within the Dirac regime and under the high-frequency approximation. We have expanded Eq. (10) to second order in Eq. (11), which will be the maximum order used here. We can, of course, obtain the Green's function $M(\mathbf{q},t)$

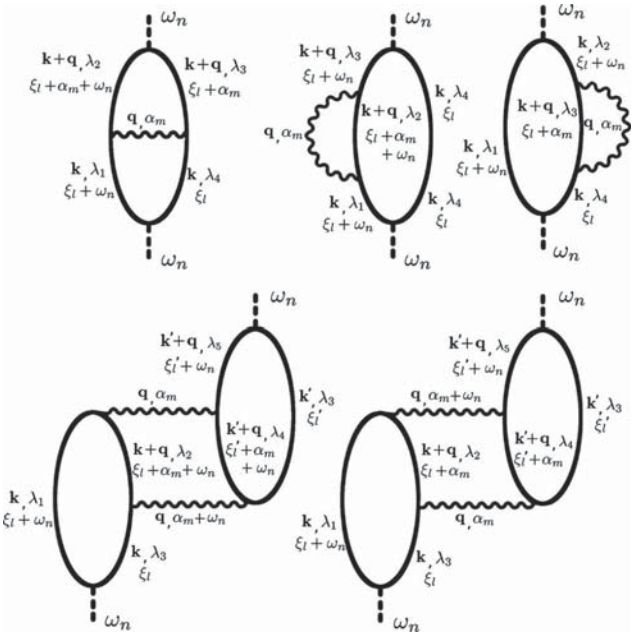

FIG. 1. The five diagrams which contribute to the high-frequency correction to the optical conductivity.

to arbitrary order of interaction. We restrict our attention to terms with equal numbers of bubbles and interaction lines which is the five diagrams given in Fig. 1. The interactions are given by the random-phase approximation (RPA) series and are shown in Fig. 2. The reason for this, aside from the desire to include screening, is that the approximation of equal numbers of bubbles and interactions is precisely fulfilled by the infinite RPA series. The effective interaction obtained via the RPA approximation is

$$V(\mathbf{q},\alpha_m) = V^0(\mathbf{q},\alpha_m) + V^0(\mathbf{q},\alpha_m)\Pi(\mathbf{q},\alpha_m)V(\mathbf{q},\alpha_m) \rightarrow V(\mathbf{q},\alpha_m) = \frac{V^0(\mathbf{q},\alpha_m)}{1 - V^0(\mathbf{q},\alpha_m)\Pi(\mathbf{q},\alpha_m)}. \tag{13}$$

Here $\Pi(\mathbf{q},\alpha_m)$ is the electronic polarizability given by

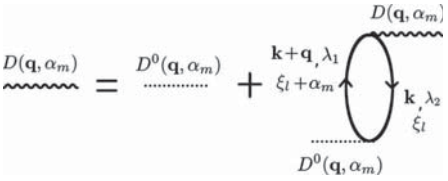

FIG. 2. The effective interaction is given by the bare phonon propagator plus an intermediate electron-phonon interaction, which causes a density fluctuation described by the electron propagator loop, followed by an effective interaction. This diagram describes the infinite sum implied by Eqs. (13) and (15). Taking the effective interaction to be of this form is equivalent to adopting the RPA approximation.

$$\Pi(\mathbf{q},\alpha_m) = \sum_{\mathbf{k},s,s'} \frac{|\langle \mathbf{k}+\mathbf{q},s'|\mathbf{k},s\rangle|^2[n_F(\epsilon_{\mathbf{k}+\mathbf{q},s'}) - n_F(\epsilon_{\mathbf{k},s})]}{\epsilon_{\mathbf{k}+\mathbf{q},s'} - \epsilon_{\mathbf{k},s} - \alpha_m}. \tag{14}$$

In Eq. (13) $V^0 = M^2 D^0(\mathbf{q},\alpha_m)$, where D^0 is the bare phonon propagator given by $D^0(\mathbf{q},\alpha_m) = \frac{2\omega_{\mathrm{LO}}}{\alpha_m^2 - \omega_{\mathrm{LO}}^2}$ for the LO branch. The effective interaction from Eq. (13) can then be written as

$$V(\mathbf{q},\alpha_m) = \frac{2\omega_{\mathrm{LO}}}{\alpha_m^2 - \omega_{\mathrm{LO}}^2 - 2\omega_{\mathrm{LO}}\Pi(\mathbf{q},\alpha_m)}. \tag{15}$$

Using the five diagrams from Fig. 1, we obtain five separate correlation functions such that Eq. (11) can be written as $M(\mathbf{q},t) = \Sigma_i^5 M^i(\mathbf{q},t)$, where the index i corresponds to the five diagrams from Fig. 1 and in terms of bare Green's functions are written as (listed according to the figure from left to right, top to bottom)

$$M^{(1)}(\mathbf{q},t) = \sum_{l,m} V_{\lambda_1,\lambda_2,\lambda_3,\lambda_4}(\mathbf{q},\alpha_m) G_{\mathbf{k},\lambda_1}(\xi_l+\omega_n) G_{\mathbf{k}+\mathbf{q},\lambda_2} \times (\xi_l+\alpha_m+\omega_n) G_{\mathbf{k}+\mathbf{q},\lambda_3}(\xi_l+\alpha_m) \times G_{\mathbf{k},\lambda_4}(\xi_l) F_{\lambda_1\lambda_2}(\mathbf{q}) F^*_{\lambda_4\lambda_3}(\mathbf{q}) v_{\lambda_2\lambda_3} v_{\lambda_4\lambda_1},$$

$$M^{(2)}(\mathbf{q},t) = \sum_{l,m} V_{\lambda_1,\lambda_2,\lambda_2,\lambda_3}(\mathbf{q},\alpha_m) G_{\mathbf{k},\lambda_1}(\xi_l+\omega_n) \times G_{\mathbf{k}+\mathbf{q},\lambda_2}(\xi_l+\alpha_m+\omega_n) G_{\mathbf{k},\lambda_3}(\xi_l+\omega_n) \times G_{\mathbf{k},\lambda_4}(\xi_l) F_{\lambda_2\lambda_1}(\mathbf{q}) F^*_{\lambda_2\lambda_3}(\mathbf{q}) v_{\lambda_3\lambda_4} v_{\lambda_4\lambda_1},$$

$$M^{(3)}(\mathbf{q},t) = \sum_{l,m} V_{\lambda_2,\lambda_3,\lambda_3,\lambda_4}(\mathbf{q},\alpha_m) G_{\mathbf{k},\lambda_1}(\xi_l+\omega_n) \times G_{\mathbf{k}+\mathbf{q},\lambda_2}(\xi_l) G_{\mathbf{k},\lambda_3}(\xi_l+\alpha_m) G_{\mathbf{k},\lambda_4}(\xi_l) \times F_{\lambda_3\lambda_2}(\mathbf{q}) F^*_{\lambda_3\lambda_4}(\mathbf{q}) v_{\lambda_1\lambda_2} v_{\lambda_4\lambda_1},$$

$$M^{(4)}(\mathbf{q},t) = \sum_{l,l',m} V_{\lambda_1,\lambda_2,\lambda_6,\lambda_5}(\mathbf{q},\alpha_m+\omega_n) G_{\mathbf{k},\lambda_1}(\xi_l+\omega_n) \times G_{\mathbf{k}+\mathbf{q},\lambda_2}(\xi_l+\alpha_m) G_{\mathbf{k},\lambda_3}(\xi_l) F_{\lambda_2\lambda_1}(\mathbf{q}) F^*_{\lambda_2\lambda_3} \times (\mathbf{q}) v_{\lambda_3\lambda_1} v_{\lambda_5\lambda_6} V_{\lambda_2,\lambda_3,\lambda_6,\lambda_5}(\mathbf{k},\alpha_m) G_{\mathbf{k}'+\mathbf{q},\lambda_4} \times (\xi_l'+\alpha_m) G_{\mathbf{k}',\lambda_5}(\xi_l'+\omega_n) \times G_{\mathbf{k}',\lambda_6}(\xi_l') F_{\lambda_4\lambda_6}(\mathbf{q}) F^*_{\lambda_4\lambda_5}(\mathbf{q}),$$

$$M^{(5)}(\mathbf{q},t) = \sum_{l,l',m} V_{\lambda_1,\lambda_2,\lambda_4,\lambda_5}(\mathbf{q},\alpha_m) G_{\mathbf{k},\lambda_1}(\xi_l+\omega_n) \times G_{\mathbf{k}+\mathbf{q},\lambda_2}(\xi_l+\alpha_m+\omega_n) G_{\mathbf{k},\lambda_3}(\xi_l) F_{\lambda_2\lambda_1}(\mathbf{q}) F^*_{\lambda_2\lambda_3} \times (\mathbf{q}) v_{\lambda_3\lambda_1} v_{\lambda_5\lambda_6} V_{\lambda_2,\lambda_3,\lambda_6,\lambda_5} \times (\mathbf{q},\alpha_m+\omega_n) G_{\mathbf{k}'+\mathbf{q},\lambda_4}(\xi_l'+\alpha_m+\omega_n) G_{\mathbf{k}',\lambda_5} \times (\xi_l'+\omega_n) G_{\mathbf{k}',\lambda_6}(\xi_l') F_{\lambda_4\lambda_6}(\mathbf{q}) F^*_{\lambda_4\lambda_5}(\mathbf{q}), \tag{16}$$

where the sum over subbands and momenta are implied.

Here G is the electron Green's function given by $G_{\mathbf{k},\lambda_n}(\xi_l) = \frac{1}{\xi_l - \epsilon_{\mathbf{k},\lambda_n}}$. Using this form of the electron Green's function, the l summation is readily performed by the residue theorem with simple poles. To proceed with the m summation, however, we cannot use the residue method because the interactions are dressed and so the poles are continuous. We use the method adopted by Perel and Eliashberg,[28] which leads to the relation,

$$\frac{1}{\beta}\sum_m \phi(\alpha_m)\psi(\alpha_m+\omega_n) = \frac{P}{2\pi i}\int dx H(x)\{[\phi^+(x)-\phi^-(x)]\psi^+(x+\omega_n) + \phi^+(x+\omega_n)[\psi^+(x)-\psi^-(x)]\}, \tag{17}$$

where $\phi(x)^{\pm} = \phi(x \pm i\eta)$, with $\eta \to 0$, can be any combination of products of $Q(x)$ and $V(x)$ terms, and $H(x)$ is the Bose-Einstein distribution function.

III. RESULTS AND DISCUSSIONS

We are now in a position to explicitly evaluate the Green's functions in Eq. (16) by summing over phonon and electron frequencies, and analytically continuing the photon frequencies into the upper half plane ($\omega_n \to \omega_n + i\eta$). As well as calculating the energetic part of the Green's functions, we shall also determine the matrix elements. In general, there are two types of transition matrix elements in this problem. The first is the transition between states at either end of an electron-phonon interaction. For massless Dirac fermions which have two subbands, there are $2^4 = 16$ possible matrix elements. However, due to electron-hole symmetry, this number is halved and we have eight possible terms. These can be described quite generally by

$$F_{ij}(\mathbf{q})F^*_{kl}(\mathbf{q}) = \frac{1}{2}Z_{ijkl}(1 + ije^{i\Delta}), \tag{18}$$

where $\Delta = \phi(\mathbf{k}+\mathbf{q}) - \phi(\mathbf{k})$, and we have introduced the permutative Levi-Civita-type operator $Z_{ijk\ldots} = \Re(\Im)$ if $ijk\ldots = 1(-1)$. The second kind of transition matrix is due to the absorption/emission of a photon and is the current matrix element. This term is described slightly differently as

$$v_{ij}(\mathbf{q}) = Z_{ij}je^{i\Delta}. \tag{19}$$

Armed with all the necessary terms specific to graphene, we obtain for the optical conductivity,

$$\sigma(\omega) = \sigma_0(\omega)\left[1 + \frac{I(\omega)}{\omega}\right], \tag{20}$$

where

$$I(\omega) = \int \frac{d\mathbf{q}}{(2\pi)^2}\frac{iP}{2\pi}\int dx n_B(\beta x)F(x,\mathbf{q}) \tag{21}$$

in which

$$F(x,\mathbf{q}) = 16\sum_{s,s'}\left[\frac{1}{4\pi^2}\int d\mathbf{k}\left[-(1+ss'\cos\Delta)\left[\frac{\cos\phi_{\mathbf{k}+\mathbf{q}}\cos\phi_{\mathbf{k}}}{\omega^2} + \frac{(4s'\epsilon_{\mathbf{k}}\epsilon_{\mathbf{k}+\mathbf{q}} - \omega^2)\sin\phi_{\mathbf{k}+\mathbf{q}}\sin\phi_{\mathbf{k}}}{(4\epsilon^2_{\mathbf{k}}+\omega^2)(4\epsilon^2_{\mathbf{k}+\mathbf{q}}+\omega^2)}\right] + \sin\Delta\left[\frac{\cos\phi_{\mathbf{k}+\mathbf{q}}\sin\phi_{\mathbf{k}}}{(4\epsilon^2_{\mathbf{k}}+\omega^2)} - \frac{\sin\phi_{\mathbf{k}+\mathbf{q}}\cos\phi_{\mathbf{k}}}{(4\epsilon^2_{\mathbf{k}+\mathbf{q}}+\omega^2)}\right] + \frac{1}{4}\left[\frac{(1+ss'\cos\Delta)^2\cos\phi^2_{\mathbf{k}}}{\omega^2} + \frac{\sin\Delta^2\sin\phi^2_{\mathbf{k}}}{4\epsilon^2_{\mathbf{k}}+\omega^2}\right] \times V(\mathbf{q},a+\omega)^+Q^{s's}(\mathbf{q},a+\omega)^+\right][V(\mathbf{q},a)^+Q^{s's}(\mathbf{q},a)^+ - V(\mathbf{q},a)^-Q^{s's}(\mathbf{q},a)^-] + \frac{1}{4\pi^2}\int d\mathbf{k}\left\{(1+ss'\cos\Delta) \times\left[ss'\frac{\cos\phi_{\mathbf{k}+\mathbf{q}}\cos\phi_{\mathbf{k}}}{\omega^2} - ss'\frac{(4s'\epsilon_{\mathbf{k}}\epsilon_{\mathbf{k}+\mathbf{q}}+\omega^2)\sin\phi_{\mathbf{k}+\mathbf{q}}\sin\phi_{\mathbf{k}}}{(4\epsilon^2_{\mathbf{k}}+\omega^2)(4\epsilon^2_{\mathbf{k}+\mathbf{q}}+\omega^2)} - \frac{\cos\phi^2_{\mathbf{k}}}{\omega^2}\right] + (1-ss'\cos\Delta)\sin\phi^2_{\mathbf{k}}\frac{(4\epsilon^2_{\mathbf{k}}-\omega^2)}{(4\epsilon^2_{\mathbf{k}}+\omega^2)^2} - \sin\Delta\left[\frac{\cos\phi_{\mathbf{k}+\mathbf{q}}\sin\phi_{\mathbf{k}}}{(4\epsilon^2_{\mathbf{k}}+\omega^2)} - \frac{\sin\phi_{\mathbf{k}+\mathbf{q}}\cos\phi_{\mathbf{k}}}{(4\epsilon^2_{\mathbf{k}+\mathbf{q}}+\omega^2)} - 2ss'\frac{\sin\phi_{\mathbf{k}}\cos\phi_{\mathbf{k}}}{(4\epsilon^2_{\mathbf{k}}+\omega^2)}\right]\right\} \times\{[V(\mathbf{q},a)^+ - V(\mathbf{q},a)^-]Q^{s's}(\mathbf{q},a+\omega)^+ + [Q^{s's}(\mathbf{q},a)^+ - Q^{s's}(\mathbf{q},a)^-]V(\mathbf{q},a+\omega)^+\} - \frac{1}{64\pi^4}\left\{\int d\mathbf{k}\left[\frac{(1+ss'\cos\Delta)^2\cos\phi^2_{\mathbf{k}}}{\omega^2} + \frac{(4\epsilon^2_{\mathbf{k}}-\omega^2)\sin\Delta^2\sin\phi^2_{\mathbf{k}}}{(4\epsilon^2_{\mathbf{k}}+\omega^2)^2}\right] \times\{[V(\mathbf{q},a)^+ - V(\mathbf{q},a)^-]V(\mathbf{q},a+\omega)^+Q^{s's}(\mathbf{q},a+\omega)^{+2} + [V(\mathbf{q},a)^+Q^{s's}(\mathbf{q},a)^{+2} - V(\mathbf{q},a)^-Q^{s's}(\mathbf{q},a)^{-2}]V(\mathbf{q},a+\omega)^+\}\right\}^2\right], \tag{22}$$

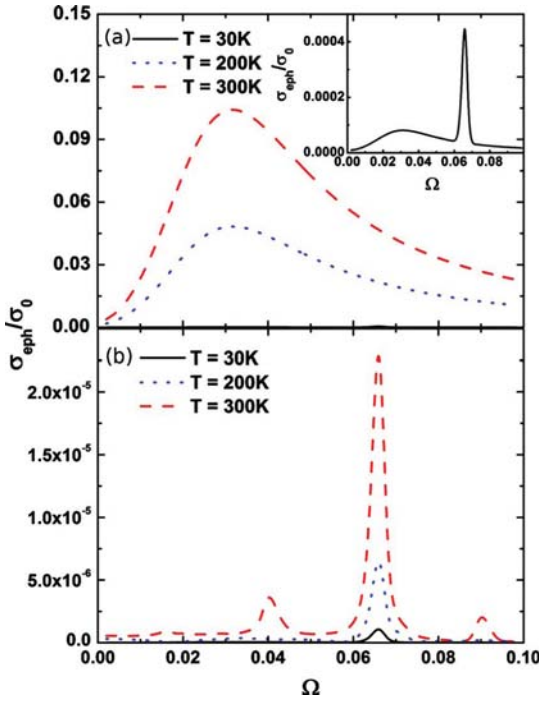

FIG. 3. (Color online) The electron-phonon-scattering-mediated conductivity of graphene ($\Omega=\hbar\omega/t$). In (a), we present both the intraband and the interband contributions. It is found that for $T>100$ K, the intraband contributions dominate. The $T=30$ K results are shown in the inset due to their relatively small magnitude. In (b), we show the interband part which is shown to have several multiphonon processes but the magnitude of this contribution is relatively negligible except at very low and very high temperatures.

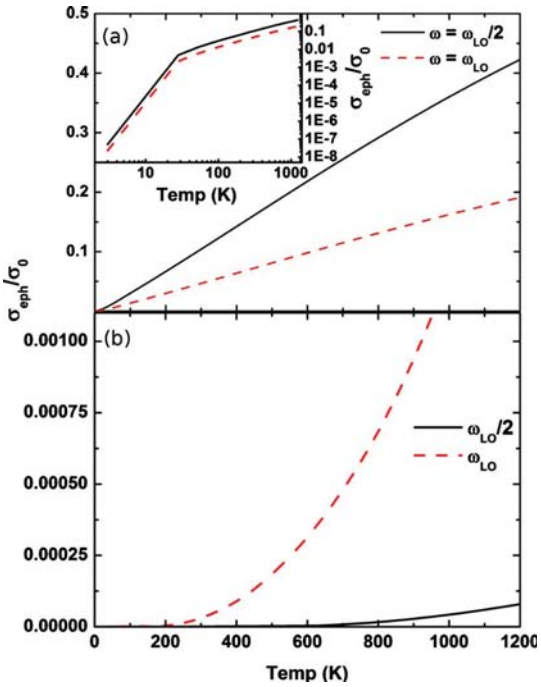

FIG. 4. (Color online) The temperature dependence of the magnitude of the conductivity at $\omega=\omega_{\mathrm{LO}}/2$ (the continuum peak) and $\omega=\omega_{\mathrm{LO}}$, (the dominant resonant peak) from Fig. 3. In (a), we show interband and intraband contributions together and obtain a roughly linear relationship. When plotted in log-log form (inset), we see that there is a significant "kink" at $T\approx 30$ K. When considering only interband transitions as in (b), both peaks display an exponential temperature dependence.

where

$$Q^{s's}(\mathbf{q},a)=\frac{n_F(\epsilon_{\mathbf{k}+\mathbf{q},s'})-n_F(\epsilon_{\mathbf{k},s})}{\epsilon_{\mathbf{k}+\mathbf{q},s'}-\epsilon_{\mathbf{k},s}-a}. \tag{23}$$

The form given by Eq. (22) is cumbersome but readily calculated numerically. The electron-phonon interaction strength for LO phonons is well known, and is given by $M^2\approx 0.035/4$ for small q, in our dimensionless units, which are normalized by v_F.[29]

In Fig. 3, we present the correction to the optical conductivity as a function of frequency, which can be attributed to scattering by screened electron-phonon interactions. Note the x axis is in the dimensionless units $\Omega=\hbar\omega/t$. First, we point out that the difference between the screened results and the unscreened results is negligible. Therefore, the effective interaction given in Eq. (15) can be approximated by the bare electron-phonon interaction with almost no loss of precision. The spectra contains both interband and intraband terms. For an intrinsic sample, these are characterized by a resonant and continuous spectrum, respectively.

Both the continuum (intraband) and resonant (interband) spectra are shown in Fig. 3(a). The 30 K results are shown in the inset due to their low magnitude. At 30 K, it can be seen that the primary interband term ($\omega=\omega_{\mathrm{LO}}$) is relatively strong but the multiphonon processes are negligible. For temperatures >100 K, the continuum results dominate so strongly that the resonant terms cannot be seen. At room temperature, it can be seen that the correction to the universal conductivity due to electron-phonon scattering is as much as $0.2\sigma_0$. The resonant (interband) spectrum is shown in Fig. 3(b), and contains terms at $\omega=n\omega_{\mathrm{LO}}/3$, where $n=[1,4]$. The $n=1$ peak is barely noticeable in the figure but can become quite prominent at higher temperatures. However, the magnitudes in Fig. 3(b) are negligible with the continuum spectrum shown in Fig. 3(a) vastly dominating for all but the lowest ($T<100$ K) and highest ($T>500$ K) temperatures.

The temperature dependence of the continuum and resonant peaks at $\omega=\omega_{\mathrm{LO}}/2$ and $\omega=\omega_{\mathrm{LO}}$, respectively, is shown in Fig. 4. It can be seen in (a) that with increasing temperature, there is an increased phonon population that facilitates both intraband and interband transitions, and so the relationship is roughly linear with increasing temperature. In the inset of Fig. 4(a), we show the log-log relationship of the same data, and it can be seen that there is a significant kink at $T\approx 30$ K, above which the roughly linear increase slows somewhat. In Fig. 4(b), we present the temperature dependence of the interband part of the same two dominant peaks. It can be seen that the resonant peak at $\omega=\omega_{\mathrm{LO}}$ increases exponentially with temperature, with the interband part of the continuum peak doing the same, only much more slowly. The interband transitions then, follow an exponential increase in transition rates whereas the intraband transitions

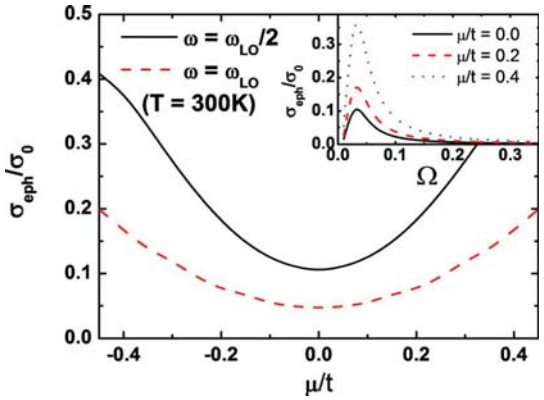

FIG. 5. (Color online) The two dominant response peaks increase in magnitude for doped samples and are symmetric about zero doping due to electron-hole symmetry. This can be attributed to the increased availability of intraband transitions, which are the dominant mechanism. In the inset, we show the full frequency dependence ($\Omega=\hbar\omega/t$) at room temperature, for three chemical-potential values. The qualitative result is unchanged by doping but the magnitudes are. This is not unexpected due to the linear subband structure.

(which are the most dominant) are roughly linear. This explains the condition that interband terms dominate at both high and low temperatures as the linear relationship will, in general, cross the exponential one at two distinct points.

It is worth noting that the qualitative behavior of the phonon-scattering-mediated conductance is similar at different doping levels. The continuum and resonant structures are essentially identical, however the interband terms also adopt a continuum as well as a resonant structure at finite doping. This is due to the peculiar gapless and linear band structure of low-energy graphene. The doping dependence of the continuum and resonant peaks are shown in Fig. 5, and are not surprisingly shown to increase with increasing doping magnitude. This is due to the extra availability of intraband transitions. Due to electron-hole symmetry, the doping dependence is symmetric about $\mu=0$. The full frequency dependence at various chemical potentials is shown in the inset of Fig. 5. We notice that the response behavior remains qualitatively identical regardless of the doping level but the magnitudes vary as explained above. Again this is not surprising, as the subband structure is linear and so somewhat self-similar at different doping levels.

IV. CONCLUSION

In this work, we have studied the effect of electron-LO-phonon interaction on the high-frequency conductivity of graphene in the regime of massless Dirac fermion. The correction due to the LO-phonon scattering to the universal optical conductivity of graphene has been calculated which can be as much as 20% at room temperature. The scattering conductivity is dominated by a continuum intraband spectrum which displays a peak at $\omega=\omega_{\mathrm{LO}}/2$. We have found that the effect of screening (within the RPA approximation) is insignificant, and that the electron-phonon interaction can be approximately described by a bare phonon propagator. This greatly simplifies calculations and is in good agreement with the dominant consensus within the field.

It was noted that there are also resonant interband terms observed at $\omega=n\omega_{\mathrm{LO}}/3$, where $n=[1,4]$, which represent single-phonon and multiphonon processes. The single-phonon process $\omega=\omega_{\mathrm{LO}}$ is dominant over the continuum results only at $T<50$ K, beyond which the continuum results vastly dominate. However, it should be noted that the results for $T<50$ K are extremely small, at around $\sigma_0/1000$ or less.

The temperature and doping dependence of these results was also investigated, and it was found that the spectra scale roughly linearly with increasing temperature, and also increase with doping magnitude. The doping dependence was found to be symmetric about $\mu=0$ due to electron-hole symmetry.

In conclusion, we have presented a qualitative and quantitative result on the electron-LO-phonon interaction in graphene under the massless Dirac fermion approximation. The temperature and frequency dependence of the electron-LO-phonon-scattering-mediated conductivity has been obtained and various multiphonon processes have been identified.

ACKNOWLEDGMENT

This work was supported in part by the Australian Research Council.

[1] K. S. Novoselov, A. K. Geim, S. V. Morozov, D. Jiang, Y. Zhang, S. V. Dubonos, I. V. Grigorieva, and A. A. Firsov, Science **306**, 666 (2004).
[2] A. K. Geim and K. S. Novoselov, Nature Mater. **6**, 183 (2007).
[3] K. S. Novoselov, A. K. Geim, S. V. Morozov, D. Jiang, M. I. Katsnelson, I. V. Grigorieva, S. V. Dubonos, and A. A. Firsov, Nature (London) **438**, 197 (2005).
[4] Y. Zhang, Y. W. Tan, H. L. Stormer, and P. Kim, Nature (London) **438**, 201 (2005).
[5] C. Berger, Z. Song, X. Li, X. Wu, N. Brown, C. Naud, D. Mayou, T. Li, J. Hass, A. N. Marchenkov, E. H. Konrad, P. N. First, and W. A. de Heer, Science **312**, 1191 (2006).
[6] H. Suzuura and T. Ando, Phys. Rev. Lett. **89**, 266603 (2002).
[7] S. V. Morozov, K. S. Novoselov, M. I. Katsnelson, F. Schedin, L. A. Ponomarenko, D. Jiang, and A. K. Geim, Phys. Rev. Lett. **97**, 016801 (2006).
[8] D. V. Khveshchenko, Phys. Rev. Lett. **97**, 036802 (2006).
[9] V. P. Gusynin, S. G. Sharapov, and J. P. Carbotte, Phys. Rev. Lett. **96**, 256802 (2006).
[10] A. B. Kuzmenko, E. van Heumen, F. Carbone, and D. van der Marel, Phys. Rev. Lett. **100**, 117401 (2008).
[11] R. R. Nair, P. Blake, A. N. Grigorenko, K. S. Novoselov, T. J.

Booth, T. Stauber, N. M. R. Peres, and A. K. Geim, Science **320**, 1308 (2008).
[12] Z. Q. Li, E. A. Henriksen, Z. Jiang, Z. Hao, M. C. Martin, P. Kim, H. L. Stormer, and D. N. Basov, Phys. Rev. Lett. **102**, 037403 (2009).
[13] A. R. Wright, F. Liu, and C. Zhang, Nanotechnology **20**, 405203 (2009).
[14] C. Zhang, L. Chen, and Z. Ma, Phys. Rev. B **77**, 241402(R) (2008).
[15] T. Stauber, N. M. R. Peres, and A. K. Geim, Phys. Rev. B **78**, 085432 (2008).
[16] S. A. Mikhailov and K. Ziegler, J. Phys.: Condens. Matter **20**, 384204 (2008).
[17] A. R. Wright, X. G. Xu, J. C. Cao, and C. Zhang, Appl. Phys. Lett. **95**, 072101 (2009).
[18] A. A. Avetisyan, B. Partoens, and F. M. Peeters, Phys. Rev. B **79**, 035421 (2009); B. Partoens and F. M. Peeters, *ibid.* **74**, 075404 (2006).
[19] J. Cserti, A. Csordas, and G. David, Phys. Rev. Lett. **99**, 066802 (2007).
[20] D. S. L. Abergel and V. I. Fal'ko, Phys. Rev. B **75**, 155430 (2007).
[21] K. F. Mak, C. H. Lui, J. Shan, and T. F. Heinz, Phys. Rev. Lett. **102**, 256405 (2009).
[22] J. Liu, A. R. Wright, C. Zhang, and Z. Ma, Appl. Phys. Lett. **93**, 041106 (2008).
[23] A. R. Wright, J. C. Cao, and C. Zhang, Phys. Rev. Lett. **103**, 207401 (2009).
[24] A. R. Wright and C. Zhang, Appl. Phys. Lett. **95**, 163104 (2009).
[25] T. Stauber and N. M. R. Peres, J. Phys.: Condens. Matter **20**, 055002 (2008).
[26] T. Stauber, N. M. R. Peres, and A. H. Castro Neto, Phys. Rev. B **78**, 085418 (2008).
[27] G. D. Mahan, *Many-Particle Physics* (Kluwer Academic, New York, 2000), p. 165.
[28] V. I. Perel and G. M. Eliashberg, Sov. Phys. JETP **14**, 633 (1962).
[29] A. H. Castro Neto, F. Guinea, N. M. R. Peres, K. S. Novoselov, and A. K. Geim, Rev. Mod. Phys. **81**, 109 (2009).